Journal of Materials Science: Materials in Electronics (2018) 29:7971–7978
https://doi.org/10.1007/s10854-018-8800-2

Theoretical and experimental approaches to measuring mechanical properties of $Zn_{1-x}Co_xO$ binary tetrahedral bulk semiconductors

E. Asikuzun[1,2] · O. Ozturk[2,3]

Received: 27 December 2017 / Accepted: 20 February 2018 / Published online: 23 February 2018

Abstract
We prepared a $Zn_{1-x}Co_xO$ system as polycrystalline nanoparticles with various compositions ($x = 0.01$, 0.02, 0.03, 0.04, 0.05, and 0.10) using sol–gel techniques and use zinc acetate dihydrate and cobalt acetate tetrahydrate as precursors. Nanoparticles were pressed under a pressure of 4 tons for 5 min into 2 mm thick disk shaped compacts 10 mm in diameter, which were then annealed at 500 °C for 30 min under a 5B Ar atmoshpere. We carried out X-ray diffraction, scanning electron microscopy, and Vickers microhardness analyses of Co doped ZnO-based nano bulk materials in detail, focusing especially on theoretical and experimental mechanical analyses. We found that calculated values were higher than the Vickers microhardness experimental results. Doping ZnO with Co did not lead to significant changes in the *a* and *c* axes. The calculated hardness values are larger than those from the experiments. Acoording to the SEM and EDS images grain size decreases as Co doping increases and the amount of Zn decreases with Co doping, respectively.

1 Introduction

Because of the promise they show as materials for use in microelectronics, binary tetrahedral semiconductors ($A^{II}B^{VI}$ and $A^{III}B^{V}$) have attracted a lot of attention recently, as many studies have looked into their electronic, mechanical, elastic, and optical properties, which directly depend on the number of valence electrons and density of the conduction electrons [1, 2]. There have been frequent attempts to understand the effects of crystal ionicity and homopolar and heteropolar contributions on chemical bonds in $A^{II}B^{VI}$ and $A^{III}B^{V}$ type binary semiconductors. Cohen [3] proposed an empirical relationship between bond length and bulk modulus for IV, III-V, and II-VI semiconductors, and Yadav et al. [4] studied the homopolar energy gap, heteropolar energy gap, and Penn gap for some types of binary compound semiconductor. The findings of these studies are often discussed, but they are not yet sufficient as models of experimental data.

ZnO is a widely studied binary semiconductor material that is non-toxic, inexpensive, and possesses good opto-electrical properties and thermal [5, 6]. ZnO is used in multiple applications, such as lasers, light emitting diodes, short wavelength optoelectronics, sensors, and spintronics. Numerous doping materials such as Co^{+2} have been used with ZnO semiconductors to improve their structural, mechanical, optical, and electrical properties [7, 8]. In addition, there are many studies on nano structures and their properties in literature [9–15].

Sol–gel technology is common name that is given to the technique of the production such as ceramic, glass and composite materials.

- A solution is formed by combining of inorganic compounds such as metal alkoxide solution or metal powders, nitrates, hydroxides and oxides with acid and water in certain amounts.
- As a result of mixing of the solution at certain temperatures, a consecutive series of chemical reactions occur in solution and a gelation occurs by electro-chemical interactions of surface charge of particles, this gelation grows gradually and reaches all points in the system and a gel form

✉ E. Asikuzun
easikuzun@kastamonu.edu.tr

[1] Department of Metallurgy and Material Engineering, Faculty of Engineering and Architecture, Kastamonu University, 37100 Kastamonu, Turkey

[2] Research and Application Center, Kastamonu University, 37100 Kastamonu, Turkey

[3] Department of Electrical and Electronics Engineering, Faculty of Engineering and Architecture, Kastamonu University, 37100 Kastamonu, Turkey

1.1 Advantages of sol–gel method

- Chemical features of method can be controlled.
- Better homogeneity is provided compared with raw material.
- Size of powder is obtained under micron.
- The low temperatures are adequate for the production.
- Obtaining of new materials and properties is possible.
- It does not cause air pollution.

And also there are different methods used to synthesize various functional inorganic nanoparticles and its property-applications [16–23].

In this study, we investigated the structural and mechanical properties of Co^{+2}-doped ZnO binary tetrahedral nano semiconductors, analyzing microhardness, which is the basis of mechanical properties, and comparing theoretical and experimental results. Detailed information is provided in the Results and Discussions section.

2 Experimental process

We prepared a $Zn_{1-x}Co_xO$ system as polycrystalline nanoparticles with various compositions ($0.0 < x < 0.10$) using sol–gel techniques, with zinc acetate dihydrate powders (Alfa Aesar) and cobalt acetate tetrahydrate powders (Alfa Aesar) used as precursors. We used methanol and acetyl acetone as solvents to prepare a homogenous solution. After weighing at appropriate rates, we covered the beakers and stirred the precursors and solvents using a heated magnetic stirrer at 60 °C for 8 h. Once we obtained a transparent solution, we uncovered the beakers and evaporated the solutions using the heated magnetic stirrer at 60 °C until we observed. Next, we preheated the gelations at 200 °C for 5 min in air using a muffle furnace to obtain powder nanoparticles, which we then pressed into 2 mm thick disk-shaped compacts 10 mm in diameter under 4 tons for 5 min. Pressed samples were then annealed at 500 °C for 30 min under 5B argon (Ar) pressure. We labeled the samples $Zn_{0.98}Co_{0.02}O$, $Zn_{0.97}Co_{0.03}O$, $Zn_{0.96}Co_{0.04}O$, $Zn_{0.95}Co_{0.05}O$, and $Zn_{0.90}Co_{0.10}O$.

In this study, we performed X-ray diffraction (XRD) measurements with a Bruker D8 Advance X-ray powder diffractometer (Fig. 1) using $Cu - K_\alpha$ radiation in the range of $30 \leq 2\theta \leq 90°$ at a scan speed of 2°/min. Sample phase structures and lattice parameters were determined by the Bruker-EVA 10.0.1.0 analysis software and ICDD PDF2-2002 data cards. We then performed surface morphology and elemental analyses of samples using a Quanta FEG 250 scanning electron microscope (SEM) and tested the

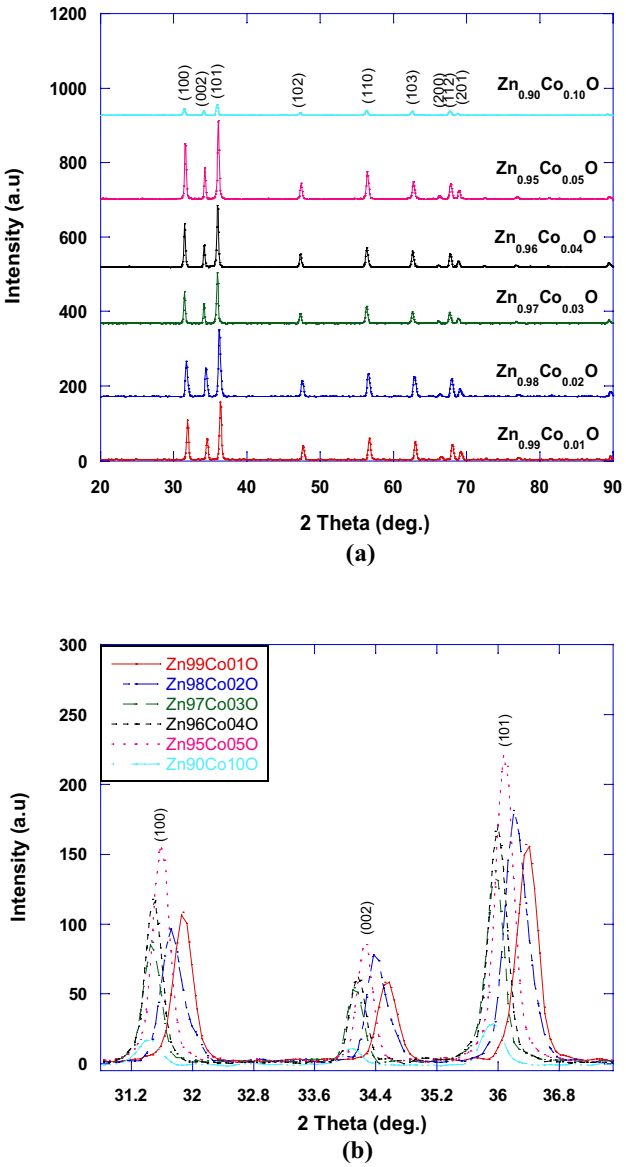

Fig. 1 XRD patterns of all nano bulk materials

mechanical characterizations of nano bulk materials using using the Vickers microhardness test with a Shimadzu brand HMV-2 model digital microhardness tester.

3 Results and discussion

We carried out XRD analyses to determine the structural quality of undoped and Co-doped ZnO based nano bulk materials. The X-ray diffraction peaks of the samples show that Co ions have no phase. This means that the presence of Co^{+2} ions in a ZnO lattice affects crystal structure becausea small amount of Co enters the structure in the lattice's grain boundary. Each sample has a hexagonal wurtzite crystal

structure that is a specific structure of Zno (ICDD Data Card No.: 01-080-0075 and 01-070-8070 for undoped ZnO and Co-doped ZnO, respectively). X-ray diffraction peaks show that the peak intensity decreases as the degree of Co doping increases (Fig. 1a). Increasing Co concentrations lead to a distortion of ZnO's crystal structure of [24]. In addition, grain size decreases as the level of Co doping increases (Table 1). Grain size is 36.95 Å for a doping rate of $x = 0.01$ and 30.99 Å for a doping rate of $x = 0.10$. In other words, peak position shifts to a smaller 2 theta angle (Fig. 1b) as Co concentration increases [25, 26], indicating that the hexagonal structure deteriorates with doping.

Lattice parameters a and c decrease slightly with Co doping, showing that Zn^{+2} ions substitute with Co^{+2} ions. There were no significant changes to average bond length (d) or α and β bond angles.

Figure 2 shows SEM images of a $Zn_{1-x}Co_xO$ bulk series, annealed under a 5-bar argon atmosphere,with a 200.000× magnification. Observing the images, we can see that grain size decreases as Co doping increases. Grain sizes are scaled during SEM measurements, but they do not very clear. We observed using this scale that grain sizes decrease with Co doping. In addition, we calculated Warren-Scherer values are calculated using XRD data, which show that grain sizes decreased the level of Co doping increased. However, the grain size of undoped ZnO increases as Co doping level increases. The size differences may be due to disparities between the ionic radii of the doping element ($Co^{+2} = 0.79$ Å) and the host element ($Zn^{+2} = 0.74$ Å). As the doping element enters the structure of ZnO, it can cause the formation of more nucleation centers [27].

The change in Zn content with Co doping is investigated by using the EDS analysis (Fig. 3). It is observed that the atomic percentage of Zn decreases with Co doping. This is an expected result. As interpreted from the XRD analysis, the Co^{+2} ions replacement with Zn^{+2} ions in the ZnO lattice due to the ionic radius of Co (0.79 Å) is greater than the ionic radius of Zn (0.74 Å). Therefore there is no peak of the Co atoms. In addition, this result is observed using EDS measurement. According the EDS analyses the amount of Zn decreases with Co doping.

Table 1 Some structural values of all nano bulk materials

Samples	a (Å)	c (Å)	Grain size (nm)	c/a
Undoped ZnO	3.74	5.22	26.71	1.40
$Zn_{0.99}Co_{0.01}O$	3.73	5.18	36.95	1.38
$Zn_{0.98}Co_{0.02}O$	3.73	5.18	36.85	1.38
$Zn_{0.97}Co_{0.03}O$	3.73	5.19	36.29	1.39
$Zn_{0.96}Co_{0.04}O$	3.73	5.19	36.14	1.39
$Zn_{0.95}Co_{0.05}O$	3.74	5.12	35.95	1.37
$Zn_{0.90}Co_{0.10}O$	3.73	5.19	23.99	1.39

ZnO has alternative Zn^{+2} and O^{-2} planes, which cause electrical polarization in the material. The size of the α angle is an important influence on polarization, and decreasing α angle causes a decrease in polarization. When an ion with an ionic radius smaller than Zn^{+2} is doped on the host material, its extra charge attracts more oxygen and provides space to accommodate the extra oxygen. In addition, doped ion groups can also cause lattice defects. Thus, Zn ions may end up in different respective positions, possibly leading to local planar defects. These local planar defects formed by doping happen when different d-spacing cause extra reflections, which are seen as extra peaks in XRD graphs. These changes also lead to alterations in the value of average bond length, d, which is associated with the free electron density parameter (r_s).

$$d = 1.173\, r_s. \tag{1}$$

In this study, we doped using Co^{+2} (0.79 Å) ions, whose ionic radius is larger than Zn^{+2} (0.74 Å). Since both ions have a +2 valence, there were no additional structural. In addition, a co-related extra diffraction peak is not observed in the XRD data (Fig. 1a). From this result, we can say that Co^{+2} ions easily displaced Zn^{+2} ions, as was predicted by the Co^{+2} ion's large ionic radius. This displacement can also be explained as Co^{+2} ions substituting Zn^{+2} ions in the ZnO host semiconductor without changing its wurtzite structure, which can be confirmed by calculating the Zn–O bond length (Table 2). There is a significant change in the α and β bond angles between Zn–Zn and Zn–O bonds. This shows that the Zn and O atoms were not moved to different positions from their original location, thus no local planar defects were formed (Table 2).

Defects and new lattice planes are instrumental in reducing energy separation (E_g), which results from homopolar and heteropolar energies. Although homopolar energy, E_h, depends on nearest neighbours distances, heteropolar energy, C, is determined by the electronegativity difference between Zn and O [28].

$$\text{Homopolar Energy}, E_h = 39.74\, d^{-2.48} \tag{2}$$

$$\text{Heteropolar Energy}, C = 98.21\left(\frac{b}{r_s}\right)e^{-\left(1.7323 r_s^{0.5}\right)} \tag{3}$$

$$b = (\Delta r)^2 + 0.03b = 0.5776 \text{ (for ZnO)} \tag{4}$$

$$\text{Avarage Energy}, E_g = \left[(E_h)^2 + (C)^2\right]^{0.5} \tag{5}$$

$$\text{İonicity}, f_i = 1 - \left(\frac{E_h}{E_g}\right)^2. \tag{6}$$

We summarized the calculated E_h, C, and E_g values in Table 2. Both the E_h and C values increased, and although there was no significant change in ionicity, the E_g tends to

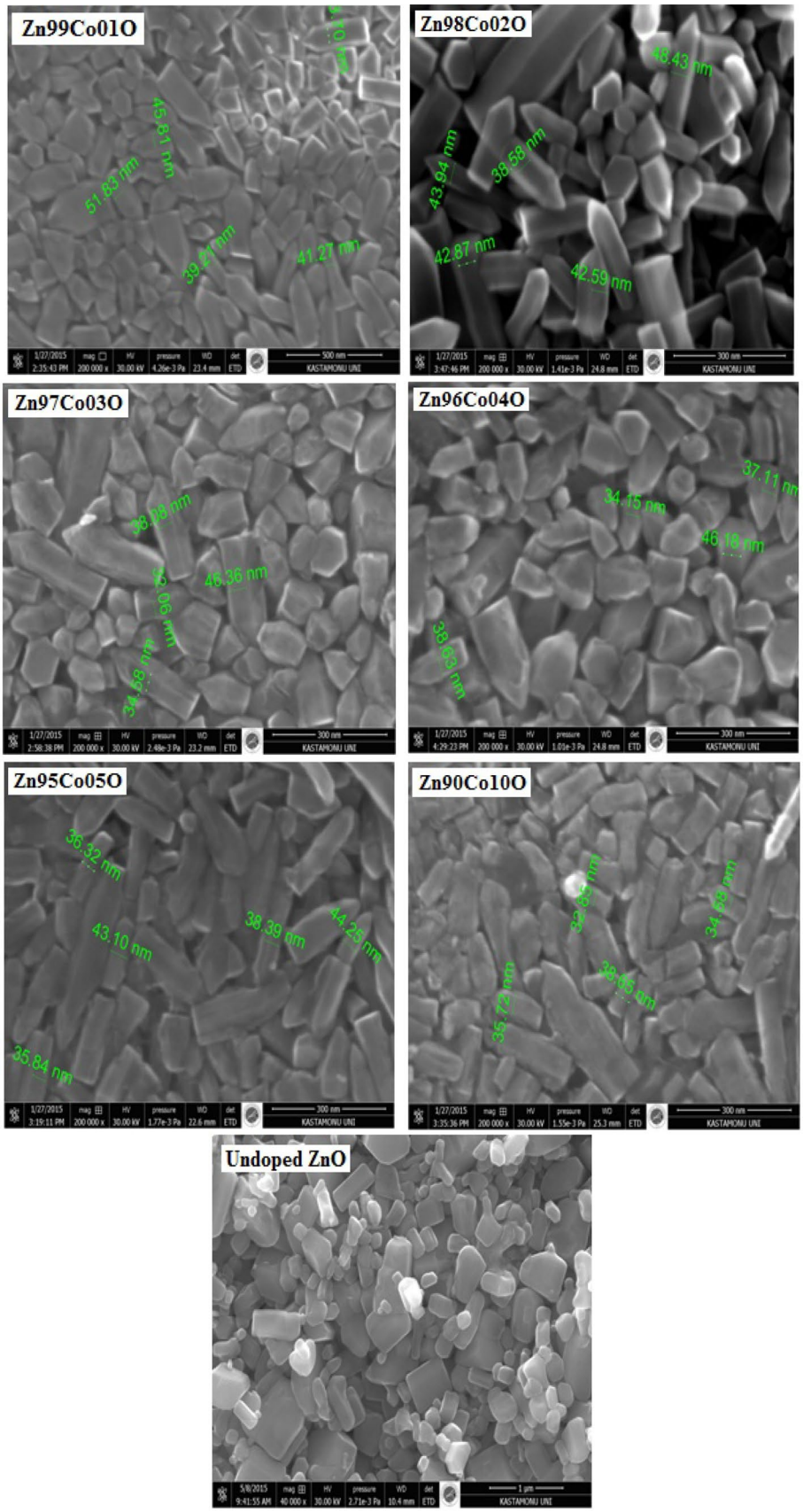

Fig. 2 SEM micrographs of all nano bulk materials

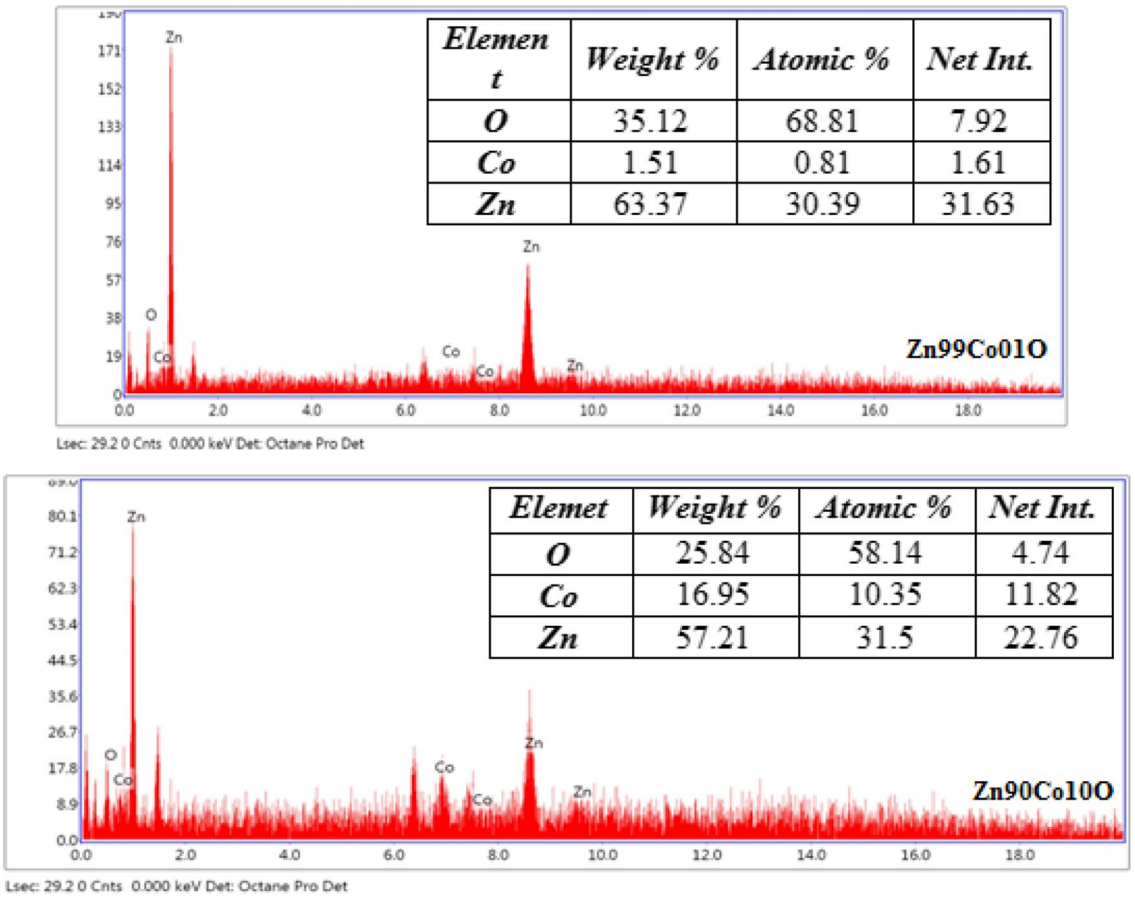

Fig. 3 EDS graphs of all nano bulk materials

Table 2 Values of energies, ionicity, average bond lengths and bond angles of all nano bulk materials

Samples	E_h	C	E_g	f_i	Average bond length (d)	α	β
Undoped ZnO	5.63	10.56	11.97	0.77	2.198	100.79	116.56
$Zn_{0.99}Co_{0.01}O$	5.68	10.60	12.03	0.77	2.190	100.51	116.73
$Zn_{0.98}Co_{0.02}O$	5.68	10.60	12.03	0.77	2.190	100.51	116.73
$Zn_{0.97}Co_{0.03}O$	5.68	10.59	12.02	0.77	2.191	100.62	116.66
$Zn_{0.96}Co_{0.04}O$	5.68	10.59	12.02	0.77	2.191	100.62	116.66
$Zn_{0.95}Co_{0.05}O$	5.68	10.60	12.02	0.77	2.190	99.70	117.20
$Zn_{0.90}Co_{0.10}O$	5.68	10.59	12.02	0.77	2.191	100.62	116.66

increase with doping (Fig. 4). The lack of change in ionicity (Table 2) may be because Co and Zn have the same valence value (+2). Compared with the undoped sample, there were no significant changes in homopolar energy or heteropolar energy with Co doping; therefore, we can say that lattice's crystallization did not deteriorate.

The materials' mechanical properties depend on the free electron density parameter, and hence, the bond length. Cohen [3] defined the bulk modulus, B, as related to bond length (d) for most binary semiconductors.

$$B = (1971 - 220\lambda)\, d^{-3.5} \tag{7}$$

where $\lambda = 2$ for II–VI group semiconductors. Hence, for ZnO we have

$$B = 1531\, d^{-3.5}. \tag{8}$$

Hardness is related to B [29].

$$B = \mu\, r_s^{(-3.5)} \tag{9}$$

where, μ is a constant with a value of 875.6 for II–VI group semiconductors and 1001.4 for III–V group semiconductors.

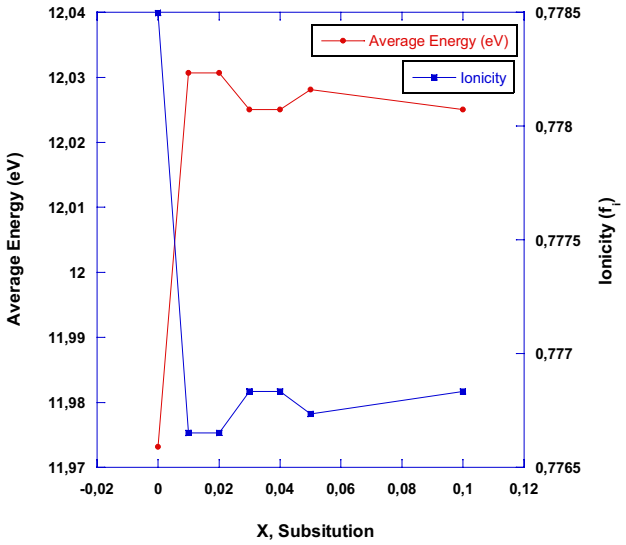

Fig. 4 Average energy and ionicity of all nano bulk materials

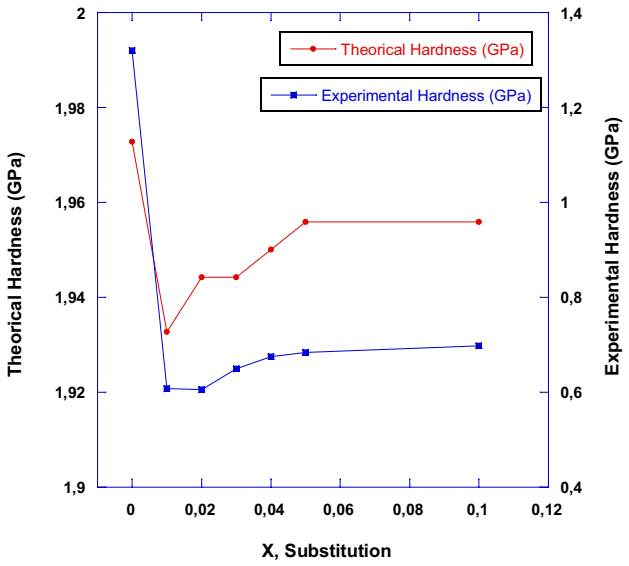

Fig. 5 Theoretical and Experimental microhardness of all nano bulk materials

Based on the above expressions, the empirical relation between H and r_S for binary tetrahedral semiconductors is:

$$H = \delta\, r_s^{(-5.57)} \tag{10}$$

where, δ is approximately 62.58 for II–VI group semiconductors.

This relation can be used to calculate the theoretical hardness of $Zn_{1-x}Co_xO$ samples. We compared these theoretical hardness values with experimental hardness values (Table 3), and found that the Vickers microhardness of samples increases with increasing Co substitution (Fig. 5).

The calculated hardness values are larger than those from the experiments, which can be explained by differences in pellet porosity. Decreasing hardness does not depend on porosity changes, because the porosity did not change. We hypothesize that decreasing the *c*/*a* ratio and improving the lattice tensile strength can cause a decrease in material hardness.

Table 3 Values of experimental and theoretical microhardness of all nano bulk materials

Samples	Experimental Vickers hardness (under 2.940 N)	Theoretical Vickers hardness	r_s
Undoped ZnO	1.320	1.973	1.86
$Zn_{0.99}Co_{0.01}O$	0.608	1.932	1.867
$Zn_{0.98}Co_{0.02}O$	0.606	1.944	1.865
$Zn_{0.97}Co_{0.03}O$	0.649	1.944	1.865
$Zn_{0.96}Co_{0.04}O$	0.675	1.950	1.864
$Zn_{0.95}Co_{0.05}O$	0.684	1.955	1.863
$Zn_{0.90}Co_{0.10}O$	0.698	1.955	1.863

3.1 Results of Vickers microhardness experimental analyses

It is known that hardness is a mechanical parameter which is related to the content and structure of the solids. Therefore, importance of the microhardness tests is increasing more and more to characterize a substance [30–33]. In this study, microhardness values are measured using a Vickers micro- hardness tester for its common usage and non-destructive measuring conditions regarding to the sample surfaces. Force is applied 300 N on the material's surface, diagonals of the trace left by the indenter are read using the microscope and load/trace area. Vickers hardness is calculated using the relation given in Eq. 11.

$$H_v = \frac{1854.4F}{d^2}\ GPa \tag{11}$$

It can be seen from Fig. 6 that the microhardness values decrease with increasing the *Co* doping level and these values increase with applied load. Microhardness values have reached the plateau (saturation region) around about 1 N for the samples.

The hardness value of the sample observed RISE behavior depends on the applied load. It shows that the indenter size is associated with applied load. This nonlinear case is named as reverse indentation size effect (RISE) in the literature [34, 35]. Smaller indentation load shows a smaller hardness value.

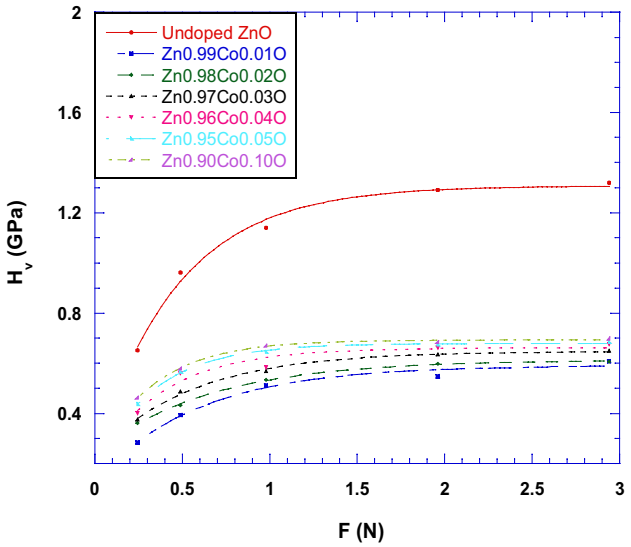

Fig. 6 The variations of experimental microhardness with load for the samples

4 Conclusions

Doping ZnO with Co did not lead to significant changes in the *a* and *c* axes. Accordingly, bond lengths and bond angles did not change. This is likely due to Zn and Co ions having the same valence values (+2). The calculated hardness values are larger than those from the experiments, which can be explained by differences in pellet porosity. Observing the SEM images, we can see that grain size decreases as Co doping increases. According the EDS analyses, there is no peak of the Co atoms and the amount of Zn decreases with Co doping.

Acknowledgements The authors would like to thank the Scientific and Technological Research Council of Turkey (TUBITAK) Project No. 114F259, the Kastamonu University Scientific Research Projects Coordination Department under the Grant No. KUBAP-05/2015-12, and Kastamonu University Research and Application Center for the supports.

References

1. A.S. Verma, R.K. Singh, S.K. Rathi, Thermal property of binary tetrahedral semiconductors. Phys. B. **404**, 4051–4053 (2009)
2. Y. Al-Douri, H. Abid, H. Aourag, Correlation between the bulk modulus and the transition pressure in semiconductors. Mater. Lett. **59**, 2032–2034 (2005)
3. M.L. Cohen, Calculation of bulk moduli of diamond and zinc-blende solids. Phys. Rev. B. **32**, 7988 (1985)
4. D.S. Yadav, S.P. Singh, Phys. Scr. **82**, 065705 (2010)
5. E. Asikuzun, O. Ozturk, L. Arda, A.T. Tasci, F. Kartal, C. Terzioglu, High-quality c-axis oriented non-vacuum Er doped ZnO thin films. Ceram. Int. **2**, 8085–8091 (2016)
6. E. Asikuzun, O. Ozturk, L. Arda, C. Terzioglu, Microstructural and electrical characterizations of transparent Er-doped ZnO nano thin films prepared by sol–gel process. J. Mat. Sci. **28**, 14314–14322 (2017)
7. E. Asikuzun, A. Donmez, L. Arda, D. Akcan, O. Ozturk, O. Cakiroglu, M. Tosun, S. Ataoglu, C. Terzioglu, Structural and mechanical properties of (Co/Mg) Co-doped nano ZnO. Ceram. Int. **41**, 6326–6334 (2015)
8. M. Tosun, S. Ataoglu, L. Arda, O. Ozturk, E. Asikuzun, D. Akcan, O. Cakiroglu, Structural and mechanical properties of ZnMgO nanoparticles. Mater. Sci. Eng. A. **590**, 416–422 (2014)
9. X. Fuku, N. Matinise, M. Masikini, K. Kasinathan, M. Maaza, An electrochemically active green synthesized polycrystalline NiO/MgO catalyst: Use in photo-catalytic applications. Mater. Res. Bull. **97**, 457–465 (2018)
10. C.M. Magdalane, K. Kaviyarasu, J.J. Vijaya, B. Siddhardha, B. Jeyaraj, Photocatalytic activity of binary metal oxide nanocomposites of CeO_2/CdO nanospheres: Investigation of optical and antimicrobial activity. J. Photochem. Photobiol. B. **163**, 77–86 (2016)
11. C. Maria Magdalane, K. Kaviyarasu, J. Judith Vijaya, C. Jayakumar, M. Maaza, B. Jeyaraj, Photocatalytic degradation effect of malachite green and catalytic hydrogenation by UV–illuminated CeO_2/CdO multilayered nanoplatelet arrays: Investigation of antifungal and antimicrobial activities. J. Photochem. Photobiol. B. **169**, 110–123 (2017)
12. K. Kaviyarasu, L. Kotsedi, A. Simo, X. Fuku, T. Genene, J. Mola, M. Kennedy, Maaza photocatalytic activity of ZrO_2 doped lead dioxide nanocomposites: Investigation of structural and optical microscopy of RhB organic dye. Appl. Surf. Sci. **421**, 234–239 (2017)
13. S.K. Jesudoss, J.J. Vijaya, P.I. Rajan, K. Kaviyarasu, M. Sivachidambaram, L.J. Kennedy, H.A. Al-Lohedan, R. Jothiramalingam, M.A. Munusamy, High performance multifunctional green Co_3O_4 spinel nanoparticles: photodegradation of textile dye effluents, catalytic hydrogenation of nitro-aromatics and antibacterial potential. Photochem. Photobiol. Sci. **16**, 766–778 (2017)
14. C. Maria Magdalane, K. Kaviyarasu, J. Judith Vijaya, B. Siddhardha, B. Jeyaraj, J. Kennedy, M. Maaza, Evaluation on the heterostructured CeO2/Y2O3 binary metal oxide nanocomposites for UV/VIS light induced photocatalytic degradation of Rhodamine—B dye for textile engineering application. J. Alloy. Compd. **727**, 1324–1337 (2017)
15. P.I. Rajan, J.J. Vijaya, S.K. Jesudoss, K. Kaviyarasu, L.J. Kennedy, R. Jothiramalingam, A. Hamad, H.A. Al-Lohedan, M.A. Vaali-Mohammed, Green-fuel-mediated synthesis of self-assembled NiO nano-sticks for dual applications photocatalytic activity on Rose Bengal dye and antimicrobial action on bacterial strains. Mater. Res. Express. **4**, 085030 (2017)
16. I. Narkeviciute, P. Chakthranont, A.J. Mackus, C. Hahn, B.A. Pinaud, S.F. Bent, T.F. Jaramillo, Tandem core–shell Si–Ta3N5 photoanodes for photoelectrochemical water splitting. Nano Lett. **16**, 7565–7572 (2016)
17. K.R. Reddy, B.C. Sin, C.H. Yoo, W. Park, K.S. Ryu, J.S. Lee, D. Sohn, Y. Lee, A new one-step synthesis method for coating multi-walled carbon nanotubes with cuprous oxide nanoparticles. Scr. Mater. **58**, 1010–1013 (2008)
18. K.R. Reddy, M. Hassan, V.G. Gomes, Hybrid nanostructures based on titanium dioxide for enhanced photocatalysis. Appl. Catal. A. **489**, 1–16 (2015)
19. Y.P. Zhang, S.H. Lee, K.R. Reddy, A.I. Gopalan, K.P. Lee, Synthesis and characterization of core-shell SiO_2 nanoparticles/poly (3-aminophenylboronic acid) composites. J. Appl. Polym. Sci. **104**, 2743–2750 (2007)

20. K.R. Reddy, K.P. Lee, A. Gopalan, Self-assembly directed synthesis of poly(ortho-toluidine)-metal(gold and palladium) composite nanospheres. J. Nanosci. Nanotechnol. **7**, 3117–3125 (2007)
21. A.M. Showkat, Y.P. Zhang, M.S. Kim, A.I. Gopalan, K.R. Reddy, K.P. Lee, Analysis of heavy metal toxic ions by adsorption onto amino-functionalized ordered mesoporous silica. Bull. Korean Chem. Soc. **28**, 1985–1992 (2007)
22. K.R. Reddy, K. Nakata, T. Ochiai, T. Murakami, D.A. Tryk, A. Fujishima, Facile fabrication and photocatalytic application of Ag nanoparticles-TiO_2 nanofiber composites. J. Nanosci. Nanotechnol. **11**, 3692–3695 (2011)
23. M. Hassan, E. Haque, K.R. Reddy, A.I. Minett, J. Chenc, V.G. Gomes, Edge-enriched graphene quantum dots for enhanced photo-luminescence and supercapacitance. Nanoscale. **6**, 11988–11994 (2014)
24. X.J. Liu, X.Y. Zhu, J.T. Luo, F. Zeng, F. Pan, Grain boundary defects-mediated room temperature ferromagnetism in Co-doped ZnO film. J. Alloys Compd. **482**, 224–228 (2009)
25. D.K. Takci, E.S. Tuzemen, K. Kara, S. Yilmaz, R. Esen, O. Baglayan, Influence of Al concentration on structural and optical properties of Al-doped ZnO thin films. J. Mater. Sci. **25**, 2078–2085 (2014)
26. O. Ozturk, M. Coskunyurek, E. Asikuzun, N. Soylu, A. Hancerliogullari, A. Varilci, C. Terzioglu, The effect of Nd_2O_3 addition on superconducting and structural properties and activation energy calculation of Bi-2212 superconducting system. J. Mater. Sci. **25**, 444–453 (2014)
27. C.Y. Tsay, W.C. Lee, Effect of dopants on the structural, optical and electrical properties of sol-gel derived ZnO semiconductor thin films. Curr. Appl. Phys. **13**, 60–65 (2013)
28. G. Bajpai, T. Srivastava, M. Nasir, S. Tiwari, S. Bajpai, E.G. Rini, S. Biring, S. Sen, A comprehensive theoretical and experimental study on structural and mechanical properties of Si doped ZnO. Scr. Mater. **135**, 1–4 (2017)
29. J.N. Plendl, S.S. Mitra, P.J. Gielisse, Compressibility, cohesive energy, and hardness of non-metallic solids. Phys. Status Solidi B. **12**, 367 (1965)
30. E. Asikuzun, O. Ozturk, H.A. Cetinkara, G. Yildirim, A. Varilci, M. Yılmazlar, C. Terzioglu, Vickers hardness measurements and some physical properties of Pr_2O_3 doped Bi-2212 superconductors. J. Mater. Sci. **23**, 1001–1010 (2012)
31. S.M. Khalil, Enhancement of superconducting and mechanical properties in BSCCO with Pb additions. J. Phys. Chem. Solids. **62**, 457–466 (2001)
32. H. Aydın, O. Cakiroglu, M. Nursoy, C. Terzioglu, Mechanical and superconducting properties of the $Bi_{1.8}Pb_{0.35}Sr_{1.9}Ca_{2.1}Cu_3Gd_xO_y$ system. Chin. J. Phys. **47**, 192–206 (2009)
33. J.B. Quinn, G.D. Quinn, Indentation brittleness of ceramics: a fresh approach. J. Mater. Sci. **32**, 4331–4346 (1997)
34. J. Gong, J. Wu, Z. Guan, Examination of the indentation size effect in low-load vickers hardness testing of ceramics. J. Eur. Ceram. Soc. **19**, 2625–2631 (1999)
35. A. Elmustafa, D. Stone, Nanoindentation and the indentation size effect: Kinetics of deformation and strain gradient plasticity. J. Mech. Phys. Solids **51**, 357–381 (2003)